Large-scale spiral structures in turbulent thermal convection between two vertical plates

Minghao Wang,* Song Fu,† and Guanghua Zhang‡
Department of Engineering Mechanics, Tsinghua University, Beijing 100084, China
(Received 15 February 2002; published 19 December 2002)

By means of a three-dimensional numerical simulation of the Boussinesq equations, it is observed that the turbulent flow induced by thermal convection between two differentially heated vertical plates can generate strongly spiral structures on large scales. In this paper, the flow patterns and the temporal evolution of such large-scale spiral structures are manifested. It is shown that the length scale of the spiral structures is comparable to the width of the convection layer and their lifetime is about two or three orders of magnitude longer than that of small-scale structures of the turbulence. To understand the physical mechanism of the emergence of such structures, a topological interpretation of generating the structures and the role of helicity in preserving the structures are investigated and discussed.

DOI: 10.1103/PhysRevE.66.066306 PACS number(s): 47.27.−i

I. INTRODUCTION

The generation of large-scale coherent structures is one of the most interesting and yet poorly understood processes in turbulent flows. Frisch *et al.* [1] found a numerical evidence that small forcing lacking isotropy and parity invariance could lead to the growth of a very strong large-scale helical flow. They attributed the emergence of this phenomenon to the large-scale instability caused by the so-called anisotropic kinetic alpha (AKA) effect. Sulem *et al.* [2] further demonstrated that these large-scale structures are generated by a mechanism of inverse cascade with successive appearance of structures of larger and larger scales and eventually the flow goes to a steady state dominated by structures of the largest available scales. Yakhot and Pelz [3] also presented their results of direct numerical simulations (DNS) showing three-dimensional inverse cascade which leads to the generation of a large-scale secondary flow by anisotropic small-scale primary flow. They explained this phenomenon as a manifestation of long-wave instability of the corresponding small-scale flow.

For the flows induced by thermal convection, most investigations have been concentrated on the Rayleigh-Bénard convection. In such cases, the Rayleigh number plays an important role in generating different types of large-scale structures. In the so-called ''soft turbulence'' regime at low Rayleigh numbers ($Ra<4\times10^7$, normally), Clever and Busse [4] reported enhanced vertical vorticity associated with the toroidal component of fluid motion, when the flow undergoes bifurcation to oscillatory knot convection. This phenomenon occurs on horizontal length scales comparable to the depth of the convection layer. In the ''hard turbulence'' regime at sufficiently high Rayleigh numbers, Cortese and Balachandar [5] investigated the vortical nature of thermal plumes through a numerically simulated Rayleigh-Bénard convection. They revealed the existence of up-moving and down-moving plumes associated with significant vertical vorticity, of which the horizontal scale is nearly an order of magnitude smaller than the layer depth. As opposed to the mechanism of large-scale instability, they proposed that the physical mechanism responsible for these different scaling structures is the interaction between the buoyancy induced vertical flow and the shear associated with the large-scale horizontal cellular motions which exist instantaneously near the top and bottom boundaries.

However, only a few published works have contributed to the understanding of the coherent structures in the thermal convection in a vertical fluid layer. Boudjemadi *et al.* [6] and Phillips [7], respectively, performed DNS studies on the natural convection between two vertical plates heated at different temperatures. But the latter case is at lower Rayleigh number ($Ra=4.6\times10^4$ and $Ra=1.28\times10^5$). The main focus was on the statistical mean flow behavior rather than on the large-scale coherent structures. Versteegh and Nieuwstadt [8] investigated the same flow through DNS with any larger

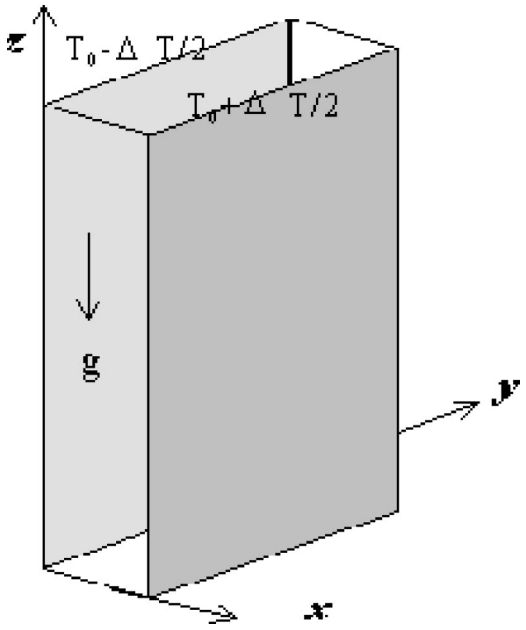

FIG. 1. Schematic of the thermal convection between two vertical plates.

*Electronic address: wmh99@mails.tsinghua.edu.cn
†Electronic address: fs-dem@mail.tsinghua.edu.cn
‡Electronic address: zhanggh@mail.tsinghua.edu.cn

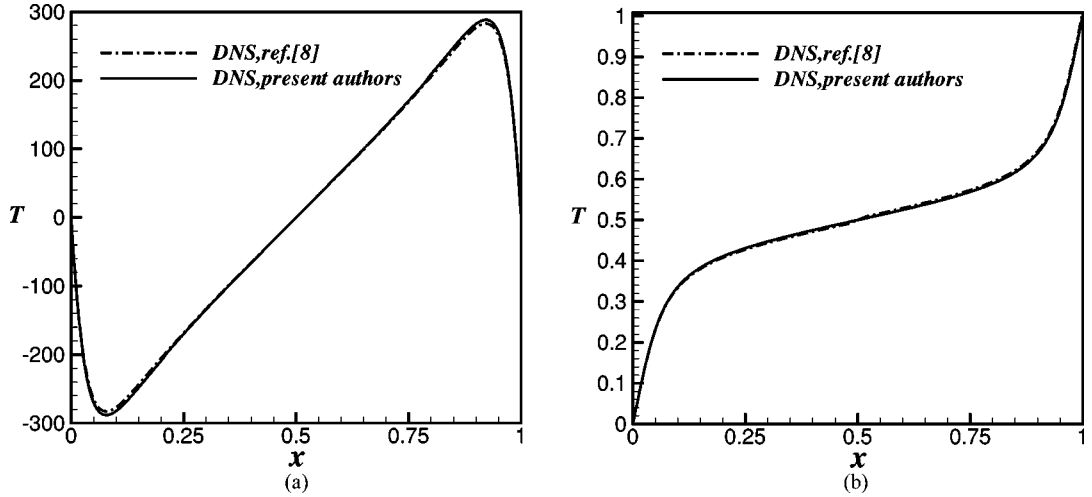

FIG. 2. Mean velocity (a) and mean temperature (b) distributions of the thermal convection flow ($\mathrm{Pr}=0.71$, $\mathrm{Ra}=5.4\times10^5$).

computational domain. It was realized in that work that better agreement with the experimental data of Dafa'Alla and Betts [9] can be achieved with the larger computational domain size. Using the DNS data, Versteegh and Nieuwstadt also studied the coherent structures present in the flow [10], and argued that the most unstable flow pattern in the transitional regime could still be recognized in the turbulent flow at a Rayleigh number in the range of 5.4×10^5 to 5.0×10^6 . In the present work, the Versteegh and Nieuwstadt's case [10] with $\mathrm{Ra}=5.4\times10^5$ is further scrutinized through DNS. It is observed that the large-scale coherent spiral structures generally occur in the thermal convection between two vertical isothermal plates kept at different temperatures (Fig. 1). The flow patterns and the temporal evolution of such large-scale spiral structures are manifested. The nature and possible physical mechanism of the emergence of such spiral structures are elucidated and discussed.

II. DIRECT NUMERICAL SIMULATION OF THE BOUSSINESQ EQUATIONS

The flow induced by the thermal convection can be described by the well-known Boussinesq equations. In the nondimensional forms they are as follows:

$$\frac{\partial u_i}{\partial x_i}=0, \tag{1}$$

$$\frac{Du_i}{Dt}=-\frac{\partial p}{\partial x_i}+\mathrm{Pr}\frac{\partial^2 u_i}{\partial x_j \partial x_j}+\mathrm{Ra}\,\mathrm{Pr}(T-T_0)\,\delta_{3i}, \tag{2}$$

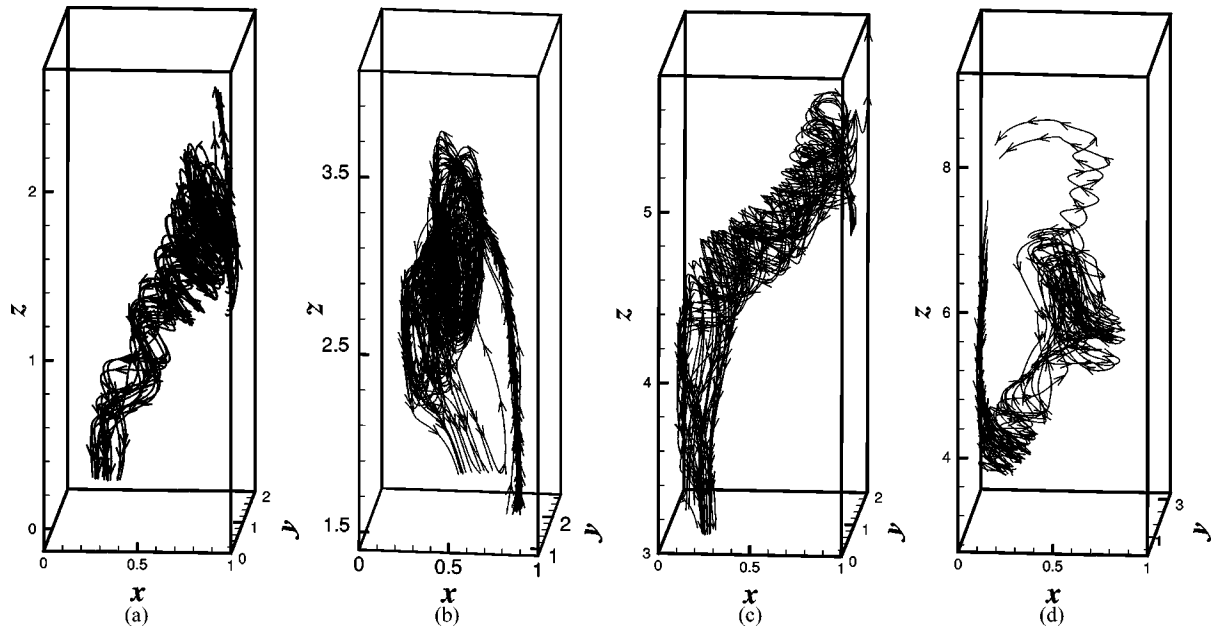

FIG. 3. Isolated instantaneous spiral structures corresponding to the high-helicity regions near the hot plate [(a), (b), (c)] and the cold plate (d) ($\mathrm{Pr}=0.71$, $\mathrm{Ra}=5.4\times10^5$), which appear in different moments, and the center points of the starting section of the structures are located, respectively, about at the coordinates of (0.95, 1, 2.4), (0.8, 2.2, 0), (0.95, 1.5, 5.6), and (0.05, 2.2, 6).

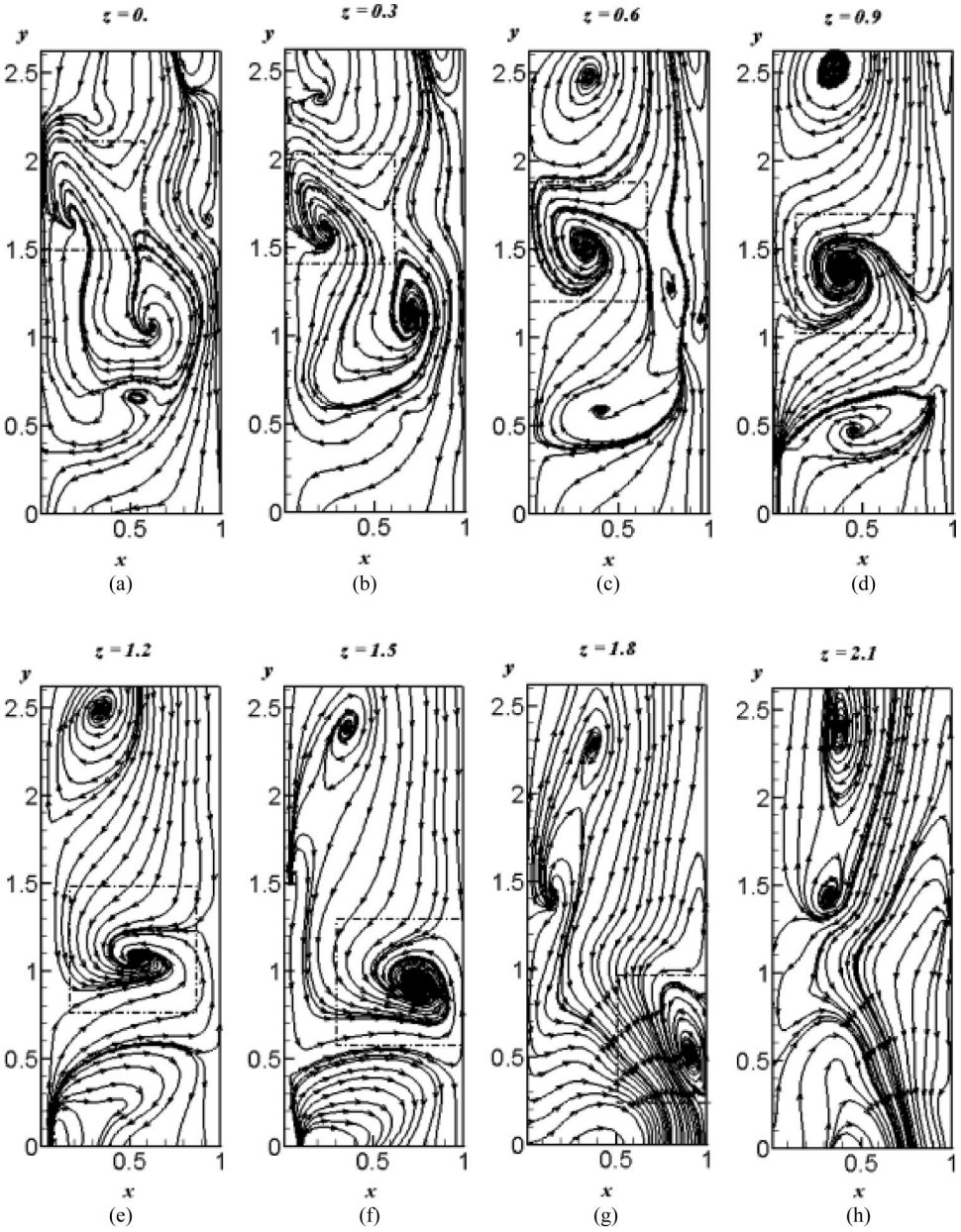

FIG. 4. Projections of the flow pattern on the planes perpendicular to the z axis. Domains enclosed with dash-dotted squares correspond to the structure given in Fig. 3(a).

$$\frac{DT}{Dt} = \frac{\partial^2 T}{\partial x_j \partial x_j}, \tag{3}$$

where $\mathrm{Ra} = \beta g \Delta T h^3 / \kappa \nu$ is the Rayleigh number, $\mathrm{Pr} = \nu / \kappa$ the Prandtl number, and h is the spacing between the two plates. The coefficients β, ν, and κ are the thermal expansion coefficient, kinematic viscosity, and thermal diffusion coefficient of the fluid, respectively. The subscript indices i and $j(=1,2,3)$ in the above equations correspond to component in x, y, z, respectively. δ_{ij} is the Kronecker delta. If Pr of the fluid is constant, then the only characteristic parameter is Ra. All the variables in this paper are nondimensionalized with h being the length scale, κ/h being the velocity scale, and h^2/κ being the time scale.

According to Ruth's instability analysis [11], the lowest critical Rayleigh number at which the flow starts to transit from laminar to turbulent state is about 5710 when Pr $=0.71$. In the present numerical simulation the Prandtl number is taken as 0.71 and $\mathrm{Ra} = 5.4 \times 10^5$. The flow is therefore well above the instability threshold. Equations (1)–(3) are solved numerically in a computational domain of the size $L_x \times L_y \times L_z = 1 \times \pi \times 2\pi$ in the normal, spanwise, and streamwise directions. For the boundary conditions, the no-slip condition is applied to the surfaces of the two vertical plates for velocity and the isotherm condition for temperature. In the homogeneous y and z direction, the flow is assumed periodic. A Cartesian grid system with the number of grid points $N_x \times N_y \times N_z = 96 \times 90 \times 206$ is adopted. In the y and z direction the grid spacing is uniform, whereas in the x direction the grid spacing is nonuniform with the minimum size near the wall and the maximum size near the centerline.

From Kolmogorov hypothesis, it is estimated that the smallest length and time scales are, respectively, 0.017 and 1×10^{-4} in the flow. The numerical technique applied here is

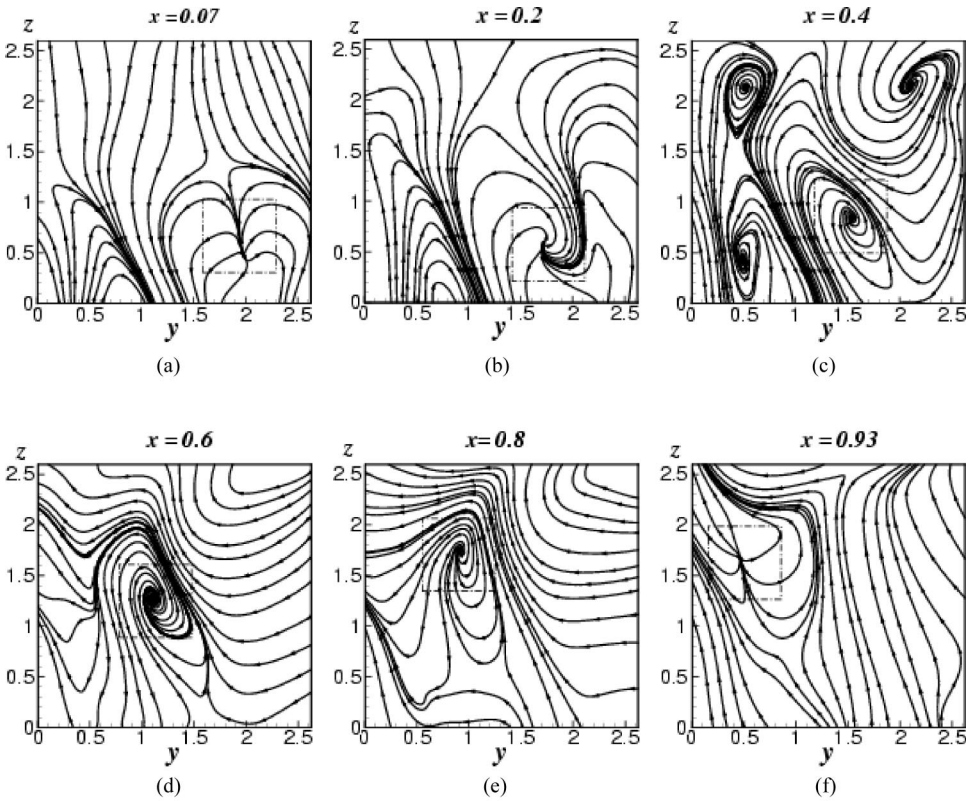

FIG. 5. Projections of the flow pattern on the planes perpendicular to the x axis. Domains enclosed with dash-dotted squares correspond to the structure given in Fig. 3(a).

a finite-volume scheme with second-order discretization for both the nonlinear advection and the viscous diffusion terms. The time-stepping method is an implicit scheme of second-order accuracy. The numerical accuracy is similar to that in Versteegh and Nieuwstadt's [8] study. It was considered that such an accuracy is sufficient for a qualitative description of the large-scale flow patterns.

After a sufficiently long time of computation starting from the initial condition, about 0.6 nondimensional time long, the flow reaches a statistically steady state. The mean velocity and mean temperature distributions of the flow are shown in Fig. 2, together with the results obtained by Versteegh and Niuwstadt [8].

In the following section we will present only the computational results associated with the instantaneous flow patterns and temporal evolution of the large-scale spiral coherent structures.

III. INSTANTANEOUS FLOW PATTERNS AND TIME EVOLUTION OF THE LARGE-SCALE SPIRAL STRUCTURES

In the present study the major observation is the spiral structures in addition to the commonly observed spanwise vortices which represent the main coherent features of the flow. In this section the helical form of the large-scale structures extracted from the database is to be illustrated describing their temporal evolution.

In order to have an intuitive impression of the large-scale spiral structures in this type of flows, Fig. 3 shows some instantaneous flow patterns represented by the streamlines passing through the high-helicity regions near the hot or cold walls. These flow structures are then examined with their projections on a series of planes perpendicular to the z axis (mean streamwise) and x axis (normal to the walls), respectively. For examples, Figs. 4 and 5 show such projections in which domains enclosed with a dash-dotted square box correspond to the flow structure of Fig. 3(a). It is seen in Fig. 4 that the spiral structure originates at the plane $z=0$ near the cold wall. At the plane $z=0$, which is the bottom cross section of the computational domain, a pair of spiral singularities exist, one being inside the square box and the other outside. These two singularities wind up to form an asymmetric counter-rotating vortex pair at the plane $z=0.3$. Meanwhile, at the plane $x=0.07$ very close to the cold wall, a singularity of skew divergent node in the square box can be observed in Fig. 5. This singularity node is strongly characterized by the upward velocity component in z direction against the general downward motion of the fluid outside the singularity region due to buoyancy effect. The strong upward motion generates large shear rates around the singularity node causing this node singularity to develop a spiral singularity which becomes evident at the plane $x=0.2$. Further away from the cold wall, i.e., at the plane $x=0.4$, a pair of asymmetric counter-rotating vortices form with one of them inside the square box as shown in Fig. 5. Upwards in z direction, as $z=0.3$–1.2, the vortex of the counter-rotating pair outside and below the square box (see Fig. 5) becomes weaker and weaker and disappears eventually. As the spiral flow reaches a position near the hot wall, the strength of the vortex highlighted in the square box degenerates again to a divergent-node singularity (see Fig. 5 for the plane $x=0.93$) denoting a transverse velocity component in x direc-

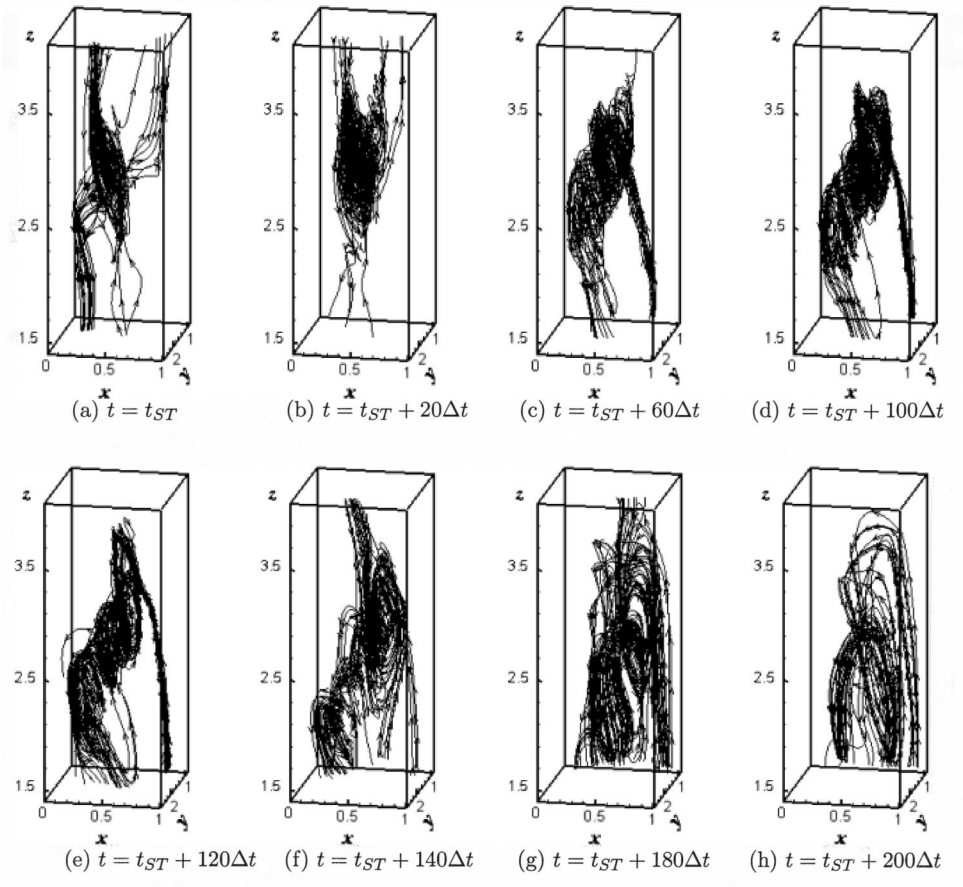

FIG. 6. Evolution of a spiral structure with time, $\Delta t = 5 \times 10^{-5}$ is the time step normalized by h^2/κ (Pr=0.71, Ra=5.4×10^5).

tion. Figure 4 thus illustrates that the spiral structure in Fig. 3(a) stretches mainly upwards tilting from the cold wall to the hot with an angle of about 21.2°.

The cause of the spiral structure from generation to disappearance is interesting and important for the investigation of its mechanism. The time evolution of the spiral structure shown in Fig. 3(b) is illustrated in Fig. 6, where t_{ST} is the starting time for observation, $\Delta t = 5 \times 10^{-5}$ is the nondimensional time increment in the DNS computation. The procedure to find such a time series is first to identify a midlife structure shown in Fig. 6(d) through searching the field values with large relative helicity at a particular instance to get a spiral structure like in Fig. 3(b). Then, the flow streamlines are plotted before and after this time until the spiral streamlines disappear. This figure thus illustrates that the lifetime of such a large-scale spiral structure is about of the same order of the global time scale defined by the characteristic length h and the friction velocity u_* [$u_* = \sqrt{\tau_w/\rho} \approx 0.011$, $\tau_w = \mu (dW/dx)|_{wall}$]. The lifetime of the helical flow pattern is equivalent to the time interval in which the flow preserves its topological structure. It is seen that this time interval is at least two orders of magnitude longer than that of small-scale turbulence structure.

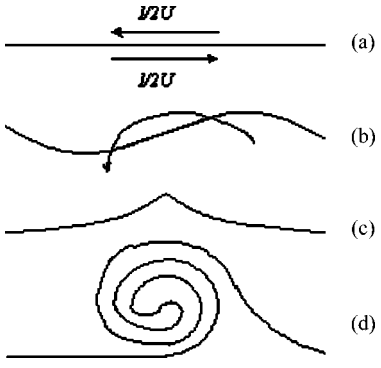

FIG. 7. Kelvin-Helmholtz instability of a plane vortex sheet (from Moffatt [12]): (a) a plane vortex sheet; (b) sinusoidal perturbation; (c) a discontinuity of curvature at a finite time t_c of order $(k\Delta U)$; (d) the vortex sheet winds up at the position of discontinuity of curvature forming a spiral singularity.

IV. QUALITATIVE INTERPRETATION OF THE GENERATION OF SPIRAL STRUCTURES

As Moffatt [12] stated, spiral structures are the eventual outcome of Kelvin-Helmholtz instability, which is an all-pervasive phenomenon associated with almost all shear flows at high Reynolds number. This argument can be shortly summarized as follows. A turbulent flow comprises a random distribution of vortex sheets and tubes, each of such structures being subjected to the local rate of strain associated with all other vortex structures. In the buoyancy-driven flow discussed here, it is obvious that vortex sheets are readily formed especially near the cold and hot walls. It is known that a plane vortex sheet is absolutely unstable to sinusoidal

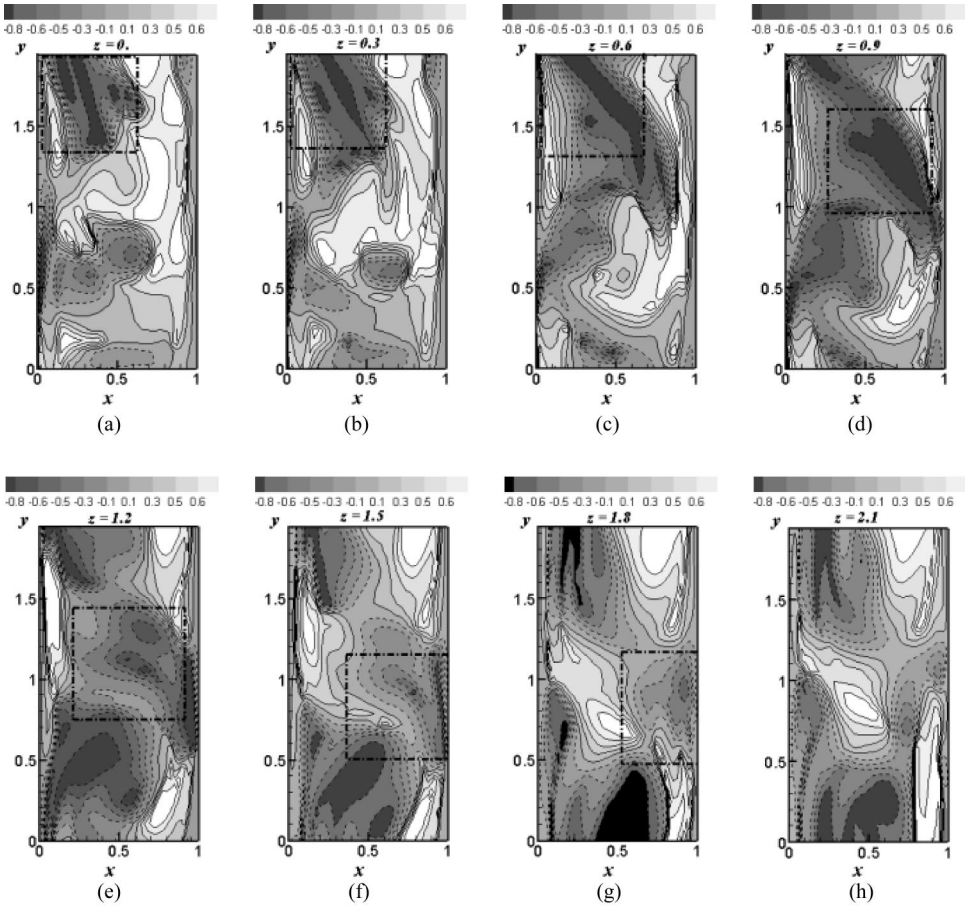

FIG. 8. Distribution of the relative helicity *h*. Domains enclosed with dash-dotted squares corresponding to the structure given in Fig. 3(b).

disturbances, and, as shown by Moore [13], the nonlinear development of an initially sinusoidal perturbation develops a mild singularity, i.e., a discontinuity of curvature, at a finite time t_c of order $(k\triangle U)$, where k is the wave number of the perturbation, and $\triangle U$ is the difference of tangential velocities on both sides of the vortex sheet. Krasny [14], who integrated the equations for vortex sheet evolution with a ''desingularisation'' procedure, demonstrated that when $t > t_c$ the vortex sheet winds up at the position of discontinuity of curvature forming a spiral singularity.

Figure 7 (from Moffatt [12]) shows the above-mentioned mechanism of Kelvin-Helmholtz instability. The spiral singularity shown in Fig. 7 is quite similar to that appears in the square box at the plane $z=0$ in Fig. 4, except that in the latter case there exists a streamwise velocity component which moves the singularity upwards to form a spiral structure.

V. ROLE OF HELICITY IN PRESERVING THE SPIRAL STRUCTURES

It has been suggested (Tsinober and Levich [15], Moffatt [16]) that the fluctuations of helicity play an important role in the nonlinear dynamics of complex flows and is likely related directly to coherent structures in turbulence. Helicity (strictly speaking helicity density) H is defined as the scalar product of the velocity and vorticity vectors, i.e., $H=\vec{u}\cdot\vec{\omega}$, where $\vec{\omega}=\nabla\times\vec{u}$. The dimensionless parameter, obtained by dividing H with the local scalar magnitudes of velocity and vorticity, is called relative helicity h, i.e., $h=H/(|\vec{u}||\vec{\omega}|)=\cos\theta$, where θ is the angle between the velocity and vorticity vectors. Both H and h are pseudoscalar quantities since they change signs if the frame of reference changes from a right-handed coordinate system to a left-handed one, in other words, H and h are quantities lacking parity invariance.

Numerical experiments (Shtilman *et al.* [17]) have shown that in regions of low energy dissipation the velocity and vorticity vectors have a tendency to align. Brandenburg and Rekowski [18] in their analysis of the energy and helicity spectra highlighted that large-scale structures supply most of the energy to the helical parts. It is conjectured that the helicity of the flow has an intrinsic property to suppress dissipation. A simple explanation is as follows. Boussinesq equation (2) can be written in its vectorial form as

$$\frac{D\vec{u}}{Dt}-\vec{u}\times\vec{\omega}=-\nabla\left(\frac{p}{\rho}+\frac{\vec{u}\cdot\vec{u}}{2}\right)+\nabla 2\vec{u}+\beta g(T-T_0)\vec{e}_3, \tag{4}$$

where $\vec{e}_3$ is the unit vector in the vertical z direction. In Eq. (4), the only nonlinear term that exchanges energy between different scales is the Lamb vector $\vec{u}\times\vec{\omega}$. This term is related to the relative helicity by an identity

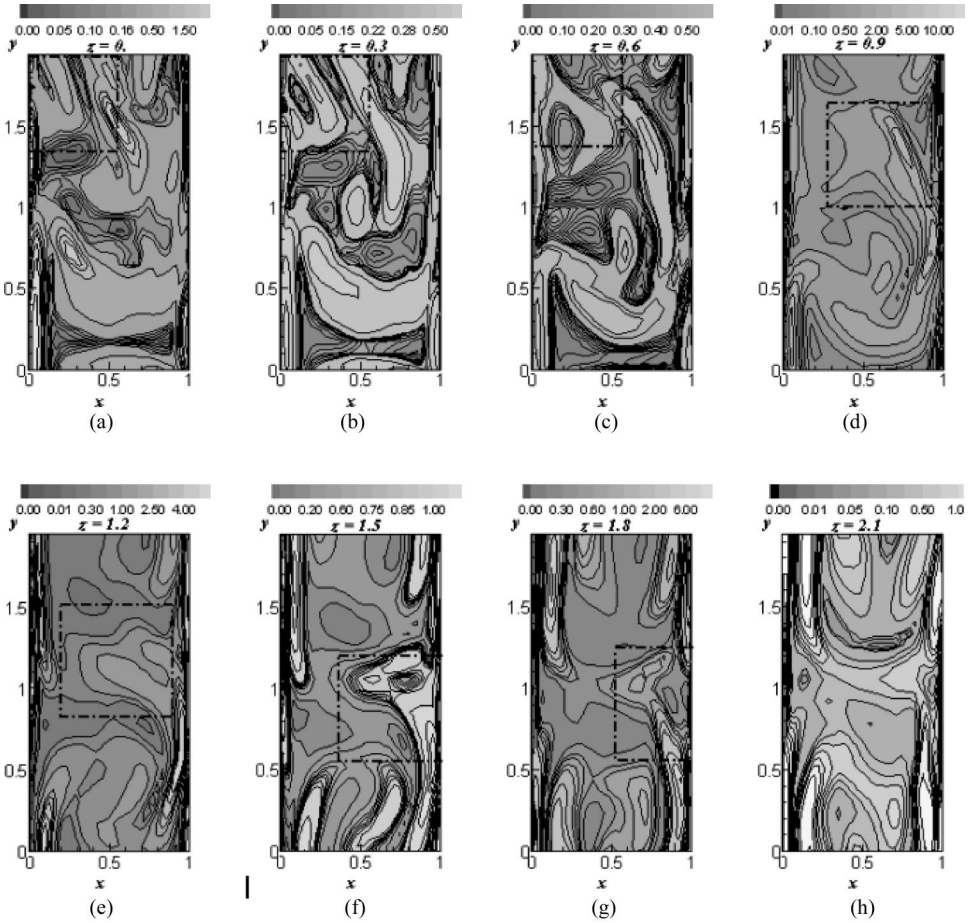

FIG. 9. Distribution of the instantaneous dissipation rate ϵ'. Domains enclosed with dash-dotted squares correspond to the structure given in Fig. 3(b).

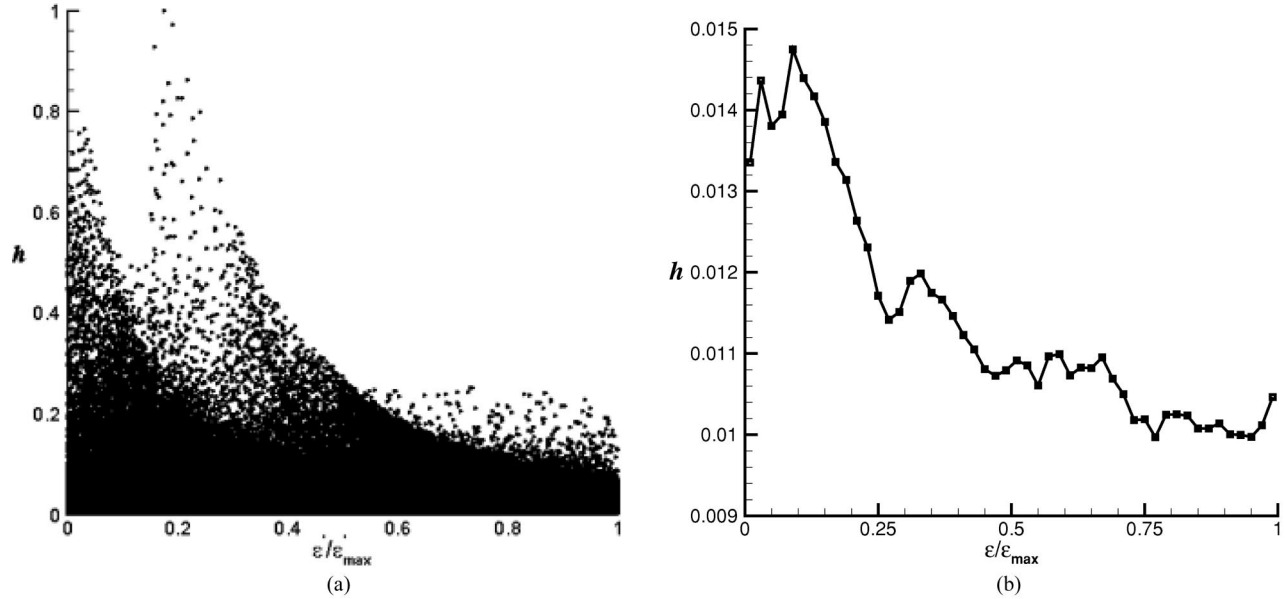

FIG. 10. (a) Dissipation rate and absolute value of relative helicity in the instantaneous flow region same as in Fig. 3(b); (b) Conditional average of relative helicity conditioned upon dissipation rate for all the computational points. The average of absolute value of relative helicity for 50 divisions from 0 to 1 with the width of 0.02 is computed for the points whose ϵ' belong to those zones.

$$\frac{|\vec{u}\times\vec{\omega}|^2}{|\vec{u}|^2|\vec{\omega}|^2}=1-h^2. \tag{5}$$

Thus, in a flow region with high helicity, the amplitude of the Lamb vector $\vec{u}\times\vec{\omega}$ is correspondingly low, and hence the energy exchange between different scales becomes less significant. A particular example is the Beltrami flow, in which $h=1$ and $|\vec{u}\times\vec{\omega}|=0$, hence, Eq. (4) becomes linear. This means that no energy transfer between different scales occurs in Beltrami flow. Generally speaking, in a high Reynolds number flow the viscous dissipation of energy-containing scales can be negligible. The removal of the energy of these scales is mainly due to nonlinear interaction and cascade behavior. This explains why a strong helical flow structure on a certain scale can preserve its energy and survive much longer than a nonhelical one.

Furthermore, if the energy cascade is suppressed by the effect of helicity, the viscous dissipation of the smallest scale would also be reduced. Thus, a flow region with high-helicity values is conjectured to correspond to that of low dissipation. The istantaneous dissipation rate ϵ' can be written as

$$\epsilon'=\nu\frac{\partial u_i'}{\partial x_j}\frac{\partial u_i'}{\partial x_j}. \tag{6}$$

Figures 8 and 9 show the distributions of relative helicity and the instantaneous dissipation rate respectively. In these figures, the flow pattern in the enclosed square boxes is related to the spiral structure, shown in Fig. 3(b). It is seen there that in the region of the spiral structure the relative helicity is large and reaches a maximum level, while the distribution of the instantaneous dissipation rate is at a relatively low level. The relationship between the helicity and the dissipation rate can be further elucidated by plotting the helicity directly against the dissipation rate as shown in Fig. 10. Figure 10(a) clearly shows that for the spiral flow indicated in Fig. 3(b), high-helicity magnitudes are closely associated with the low dissipation values. Figure 10(b) is a similar plot but with the conditional averaging over 50 equally spaced intervals in $\epsilon'/\epsilon'_{max}$. These plots confirm the conjecture metioned above. The other structures are also analyzed in similar ways, the same conclusion has also been drawn.

VI. CONCLUDING REMARKS

(1) By means of the DNS of Boussinesq equations, it is observed that the turbulent flow induced by the thermal convection between two differentially heated vertical plates can generate large-scale spiral structures. The length scale of such spiral structures is comparable to the width of the convection layer and their lifetime is about two or three orders of magnitude longer than that of small-scale structures of the turbulence.

(2) The physical mechanism of the formation of such large-scale spiral structures can be attributed to the Kelvin-Helmholtz instability, which leads to spiral singularities on a vortex sheet. The spiral singularities are then stretched by the fluid motion in the direction of the vortex axis causing the eventual formation of the large-scale spiral structures.

(3) The role of helicity in the flow is to suppress the energy cascade of turbulence, reducing the enstrophy production, and hence preserving the topological structure of the large-scale spiral flow for a significantly long time interval.

[1] U. Frisch, Z.S. She, and P.L. Sulem, Physica D **28**, 382 (1987).
[2] P.L. Sulem, Z.S. She, H. Scholl, and U. Frisch, J. Fluid Mech. **205**, 341 (1989).
[3] V. Yakhot and R. Pelz, Phys. Fluids **30**, 1272 (1987).
[4] R.M. Clever and F.H. Busse, J. Fluid Mech. **198**, 345 (1989).
[5] T. Cortese and S. Balachandar, Phys. Fluids **A5**, 3226 (1993).
[6] R. Boudjemadi, V. Maupu, D. Laurance, and P.Le. Qur, Int. J. Heat Fluid Flow **18**, 70 (1997).
[7] J.R. Phillips, Int. J. Heat Mass Transf. **39**, 2485 (1996).
[8] T.A.M. Versteegh and F.T.M. Nieuwstadt, Int. J. Heat Mass Transf. **42**, 3673 (1999).
[9] A.A. Dafa'Alla and P.L. Betts, Exp. Heat Transfer **9**, 165 (1996).
[10] T.A.M. Versteegh and F.T.M. Nieuwstadt, in Proceedings of the International Symposium on Turbulence and Heat and Mass Transfer, Delft, 1997, edited by K. Hanjalic and T.W.J. Peeters (unpublished).
[11] D.W. Ruth, Int. J. Heat Mass Transf. **22**, 1199 (1979).
[12] H.K. Moffatt, in *New Approaches and Concepts in Turbulence*, edited by Th. Dracos and A. Tsinober (Birkhäuser Verlag, Basel, 1993), pp. 121–129.
[13] D.W. Moore, Proc. R. Soc. London, Ser. A **365**, 105 (1979).
[14] R. Krasny, J. Comput. Phys. **65**, 292 (1986).
[15] A. Tsinober and E. Levich, Phys. Lett. **99A**, 321 (1983).
[16] H.K. Moffatt, in *Turbulence and Chaotic Phenomena in Fluids*, edited by T. Tatsumi (Elsevier, New York, 1984), pp. 223–230.
[17] L. Shtilman, E. Levich, S.A. Orszag, R.B. Pelz, and A. Tsinober, Phys. Lett. **113A**, 32 (1985).
[18] A. Brandenburg and B.V. Rekowski, Astron. Astrophys. **379**, 1153 (2001).